Mars' External Magnetic Field as Seen from the Surface with InSight

A. Mittelholz[1], C. L. Johnson[2,3], M. Fillingim[4], R. E. Grimm[5], S. Joy[6], S. N. Thorne[2], W. B. Banerdt[7]

[1]Department of Earth and Planetary Sciences, Harvard University, Cambridge, MA, USA.
[2]Department of Earth, Ocean and Atmospheric Sciences, The University of British Columbia, Vancouver, Canada.
[3]Planetary Science Institute, Tucson, Arizona, USA.
[4]Space Sciences Laboratory, University of California, Berkeley, USA.
[5]Southwest Research Institute, Boulder, USA.
[6]Department of Earth, Planetary, and Space Sciences, University of California, Los Angeles, USA.
[7]Jet Propulsion Laboratory, California Institute of Technology, Pasadena, USA.

Key Points:

- InSight's magnetometer provides the first surface recordings of the martian magnetic field environment over 1241 sols.
- Transient and periodic external fields with time scales of minutes up to a year are observed and their origins discussed.
- Time variations in the surface magnetic field are primarily driven by the ionosphere, affected by atmospheric seasonal variations.

Corresponding author: Anna Mittelholz, amittelholz@fas.harvard.edu

Abstract

The magnetometer of the InSight mission operated on the martian surface from November 2018 until May 2022. Previously, satellites have provided information on the martian magnetic field environment from orbit, however, the degree to which external fields penetrate to and interact with the surface could not be studied prior to the InSight landing. Here, we present an overview of the complete surface magnetic field data from InSight sols 14 to 1241 that display different external magnetic field phenomena, transient and periodic. Periodic observations range from short period waves (100s-1000s of seconds), diurnal variations, ∼26 sol Carrington rotations, to seasonal fluctuations. Transient events are observed in response to space weather and dust movement. We find that ionospheric variations are the dominant contribution as seen from the surface, while contributions from the undisturbed IMF are more subtle. We discuss limitations associated with a single point measurement and opportunities that future missions could enable. Including magnetometers on future missions at a variety of locations for long-duration continuous observations will be of great value in understanding a range of external field phenomena and will enable further investigations in different crustal magnetic field settings.

Plain Language Summary

The magnetometer of the InSight mission has measured the magnetic field at the planetary surface for the first time. Although satellites previously sampled the magnetic field globally from orbit, InSight enables a local view from the surface. Here we focus on time-varying magnetic fields driven by the Sun and the uppermost region of the atmosphere (the ionosphere); this includes the interplanetary magnetic field (IMF) and the ionosphere interacting with the planet. A range of physical phenomena can be observed. Some of those are periodic, such as the diurnal signature or seasonal variations, some are transient, such as the effect of space weather. We find that ionospheric variations are the dominant signal at the surface. We discuss limitations of such observations due to the single point measurement and possibilities future missions will provide.

1 Introduction

InSight, Interior Exploration using Seismic Investigations, Geodesy and Heat Transport, landed on Mars in Elysium Planitia at 4.5°N and 135.6°W in November 2018. The mission's primary goal is to study the interior of Mars (Banerdt et al., 2020), using observations made by the main science instruments: a seismometer, a heatflow probe and radio antennas. The InSight Fluxgate (IFG) magnetometer is part of the Auxiliary Payload Sensor System (APSS; (Banfield et al., 2018)), that was included to characterize environmental conditions around the lander to which the seismometer is sensitive. As such, the IFG is not a primary science instrument; it is however the first surface magnetometer on Mars' surface and has been providing unprecedented scientific information on the martian magnetic field environment (Johnson et al., 2020).

The IFG measures the vector magnetic field, that comprises contributions from internal and external magnetic fields, as well as from the lander itself. The latter are estimated and subtracted from the data as part of the calibration process that has been discussed elsewhere (Joy et al., 2019; Mittelholz, Johnson, Thorne, et al., 2020; Russell & Joy, 2020). Internal fields are generated below the planetary surface and result from remanent crustal magnetization acquired in an ancient field, initially detected from orbit by the Mars Global Surveyor (MGS) spacecraft (Acuna et al., 1999). External magnetic fields are generated by sources above the planetary surface, such as the ionosphere or the interplanetary magnetic field (IMF). InSight's findings related to the crustal magnetic field have been detailed previously (Johnson et al., 2020). We provide a brief summary here as context for the environment in which external fields are measured, and focus on the latter in this paper.

The InSight landing site is in a region of moderately-strong magnetized crust compared with other regions on Mars as seen from orbit (Smrekar et al., 2018; Langlais et al., 2019; Mittelholz et al., 2018). IFG data have shown that the surface magnetic field intensity is about 2000 nT, ∼10 times stronger than predicted from orbital measurements. This indicates the presence of magnetization at spatial scales smaller than ∼150 km (Johnson et al., 2020), the lowest orbital altitudes of satellite measurements from the Mars Atmosphere and Volatile Evolution (MAVEN) mission (Jakosky et al., 2015). The minimum magnetization required to explain magnetic field observations is consistent with an ancient dynamo field with Earth-like strength (Johnson et al., 2020) and could support an early (∼4 Ga) (Acuna et al., 1999; Lillis et al., 2013; Vervelidou et al., 2017), a late (Schubert et al., 2000) or a continuous or interrupted, long-lived dynamo (Mittelholz, Johnson, Feinberg, et al., 2020), depending on the buried unit(s) that carry the magnetization (Johnson et al., 2020; Knapmeyer-Endrun et al., 2021; Wieczorek et al., 2022).

External time varying magnetic fields comprise the rest of the naturally-occurring signal, and result from time-dependent processes in the overall Martian magnetic environment (Figure 1). The solar wind in which the IMF is embedded is decelerated from supersonic to subsonic velocities at the bow shock due to the martian obstacle. IMF field lines drape around the planet, and are compressed below the bowshock (Nagy et al., 2004). The magnetic pileup boundary (MPB) separates the upper magnetosheath (MS), a region with strong wave activity, from the lower magnetic pileup region. Solar photons (UV and X-rays) and energetic particles in the solar wind ionize the neutral atmosphere especially on the day-side to build up the ionosphere. Ionospheric pressure and crustal magnetic fields help to stand off the solar wind from the surface.

As a result of this magnetic field environment, periodic and transient magnetic fields driven by different mechanisms can be expected (Table 1). Those mechanisms are related to the IMF and the solar wind itself, or the ionized part of the planetary atmosphere, the ionosphere. The planet's rotation in the solar wind leads to diurnal fluctuations, and enhanced fields during the day-time. The annual cycle is driven by Mars' eccentric orbit around the Sun and associated change in dynamic pressure, and the tilt of its rota-

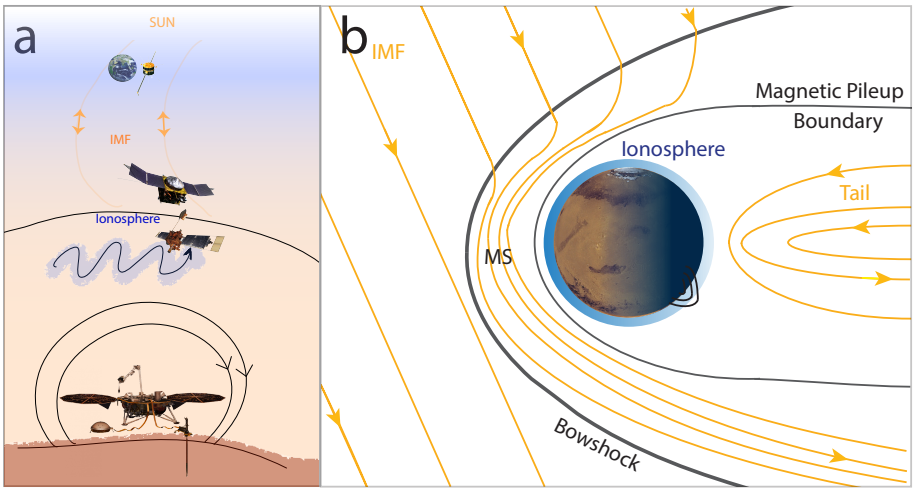

Figure 1. (a) Cartoon of the magnetic field environment as seen from InSight (b) An overview of the magnetic field environment of Mars. MS=Magnetosheath. (a)+(b) Not to scale.

tion axis resulting in more or less favourable crustal field interaction due to the concentration of the crustal fields in the Southern hemisphere. The rotation of the Sun results in a change in the position of Mars with respect to the heliospheric current sheet (i.e., above or below), and thus a polarity change of the interplanetary magnetic field at Mars every ∼13 days. At shorter periods, around 100-1000 seconds, interaction of the solar wind with the martian magnetosphere can lead to ultra low frequency (ULF) waves. Transient fields associated with solar activity, i.e. space weather, impinge on and interact with Mars' magnetosphere. Another source of time-varying fields is the ionosphere. Changes in the neutral atmosphere and/or electron density lead to diurnal, and also seasonal changes. The Sun-facing or day-side of the planet is ionized by solar photons and energetic particles, and recombination of charged particles largely neutralize this effect at the night-side, leading to diurnal magnetic field variations. Neutral winds in the atmosphere vary with season and affect currents produced in the ionospheric dynamo region. Additionally, aperiodic variations result from dust storms, that in turn have a seasonal occurrence. Dust absorbs solar radiation leading to thermal expansion of the atmosphere, raising the altitude of the entire atmospheric column including the ionosphere (Withers & Pratt, 2013), and can thus have an effect on magnetic fields at the ground resulting from ionospheric currents. In addition, local surficial dust movement can lead to triboelectric effects; the charged dust grains in suspension generate small amplitude, transient magnetic fields that are not directly related to the IMF or the ionosphere.

In the following, we focus on time varying magnetic fields as seen from the surface. To give context for these new observations we provide a short overview of satellite observations of external fields (Section 2). In Section 3 we introduce the data sets used in this paper. We show InSight IFG data collected throughout the entire mission time frame (up to sol 1241), but mainly focus on data from the first 736 sols, which provide a mostly continuous data set. In section 4, we describe surface magnetic field observations structured by period. In that section we summarize previous findings, and report new results enabled by the full time series. Lastly, we discuss the implications of observations for magnetic sounding of the planetary interior (Section 5.1) and summarize some of the open questions to motivate magnetometers on future missions to Mars (Section 5.2).

Table 1. External magnetic fields with InSight

Periodicity	**Cause**	**Detection**	**Literature**
Seasonal	Ionospheric Fluctuations; secondary: Heliospheric Distance	Yes	Mittelholz, Johnson, Thorne, et al. (2020, 2021)
Carrington Rotation	IMF	Yes	A Mittelholz et al. (2022); Luo et al. (2022)
Daily + harmonics	Ionospheric Fluctuations	Yes	Mittelholz, Johnson, Thorne, et al. (2020); Johnson et al. (2020); Luo et al. (2022)
Short - period	Interaction of Solar Wind with Mars	Yes	Chi et al. (2019); Johnson et al. (2020)
Transient: Space Weather	Transients in the Solar Wind	Yes	Mittelholz, Johnson, Fillingim, et al. (2021)
Transient: Dust Movement	Dust movement	likely, but rare	Charalambous et al. (2021); Thorne et al. (2022)

2 Brief Summary of Satellite Observations

Two satellite missions have provided magnetic field data sets at Mars (Mitteholz & Johnson, 2022): MGS (Acuna et al., 1999) and MAVEN (Jakosky et al., 2015). MGS (1997-2006) data were acquired mainly in a 400 km altitude, 2 am – 2 pm orbit around Mars. In contrast, the MAVEN orbit (2014-present) covers a variety of altitudes from approximately 135 km altitude up to above the bow shock at varying local times (Mittelholz et al., 2018). The wealth of satellite data mapping the magnetic field and plasma environment around Mars has enabled a wide range of external field studies from orbit (e.g., (Brain et al., 2003, 2006; Fillingim et al., 2010, 2012; Mittelholz et al., 2017; Ramstad et al., 2020)). We give a short summary of some key satellite-derived magnetic field observations, starting with space weather and then organized by periodicity.

Space Weather: Space weather is a generic term for transient changes in solar wind conditions and the resulting effects on interactions with planets/moons. A corotating interaction region (CIR) occurs when high speed solar wind streams originating from coronal holes overtake slower solar wind forming a region of compressed plasma. A coronal mass ejection (CME) is a large expulsion of plasma and magnetic field from the solar corona, and is referred to as an interplanetary CME (ICME) as it travels through the solar system. Depending on their propagation speed relative to the ambient solar wind speed, ICMEs can produce a shock wave in the solar wind. The velocity, density, and temperature of solar wind plasma can exhibit sharp changes at the leading edge of the ICME, followed by the strongly magnetized coronal ejecta in the ICME core, that may extend the interaction of the ICME with Mars for up to several days.

Orbital magnetic field observations of space weather at Mars come from MGS (Crider et al., 2003; Xu et al., 2019; Espley et al., 2005) and MAVEN (Jakosky et al., 2015; Luhmann et al., 2017; Lee et al., 2017, 2018; Xu et al., 2019). MAVEN's mission goal includes characterization of space weather and MAVEN's eccentric orbit which traverses the mar-

tian magnetosphere and the solar wind, in combination with the spacecraft instrument suite, is particularly suited for space weather observations. Magnetic observations are preferentially made in the IMF where the effects of space weather can usually be seen as a sudden enhancement in the field (e.g., (Jakosky et al., 2015; Lee et al., 2017, 2018)). Within the magnetosheath or pile-up region, the signature of space weather is complicated by the ionospheric response, which in turn is highly variable and dependent on local ionospheric conditions and on the complex interactions of ionospheric currents with crustal fields and the IMF. For a review of space weather observations at Mars during solar cycle 23 we refer to (Lee et al., 2017).

Annual: Magnetic field signals with annual periodicities have been observed in satellite data, but are limited by mission durations. MGS data show that peak magnetic field amplitudes tend to occur near perihelion, when Mars is closest to the Sun (Mittelholz et al., 2017). The magnetic field amplitude falls off with heliocentric distance, i.e., as $1/r$, consistent with fluid solar wind model predictions, in which the decrease in solar wind pressure with distance from the Sun is balanced by a decreased magnetic pressure (proportional to $|\mathrm{B}|^2$). The sunward component of the IMF is larger for a planet closer to the sun, where the IMF is more radial, and decreases with increasing heliocentric distance and Parker spiral angle (Figure 1a). Seasonal variability in the neutral atmosphere also leads to associated effects in the ionosphere (Lillis et al., 2019; Mittelholz, Johnson, Thorne, et al., 2020) and can alter ionospheric peak altitudes by $\pm$10 km (Morgan et al., 2008; Felici et al., 2020). During seasonally occurring dust storms, thermal expansion of the atmospheric column raises the altitude of any given isobar; because peak electron densities in the Mars ionosphere occur at a pressure of $\sim$1 nPa times the cosine of the solar zenith angle (Withers, 2009) this leads to an increase in ionospheric peak altitude for regional and large dust storms respectively (Withers & Pratt, 2013).

Solar Rotation: The solar rotation period as seen from Mars of about 26.3 days (Carrington rotation) is seen in orbital magnetic field observations as fluctuations in field strength of about 10 nT at 400 km (Brain et al., 2006; Mittelholz et al., 2017; Ferguson et al., 2005), and a polarity change in the magnetic field. At $\sim$400 km altitude the IMF can be described as a draped field and so the horizontal components dominate.

Diurnal: Diurnal periodicity in MGS data has been quantified and modeled (Mittelholz et al., 2017; Olsen et al., 2010; Ferguson et al., 2005). The difference in the average large scale structure (i.e., up to spherical harmonic degree 5 in global models) at 400 km altitude between the day side and the night-side ranges from -30 nT to 30 nT, but considerably larger fluctuations can occur on a day-to-day basis (Mittelholz et al., 2017).

Short Period Waves: Short period waves, often referred to as pulsations or ULF waves, have been attributed to compressional oscillations in the magnetotail and Kelvin-Helmholtz instabilities. These typically exhibit power in the horizontal components and range from mHz to Hz. Observations of ULF waves at Mars were made by the Phobos-2 spacecraft (Sagdeev & Zakharov, 1989) and later by other spacecraft such as MGS (Brain et al., 2002; Espley et al., 2004). Studies of the lowest segments of MGS orbits allowed identification of ULF waves at ionospheric altitudes (Espley et al., 2006). MAVEN data (Connerney et al., 2015; Harada et al., 2019) have allowed investigations of newly-identified compressional narrow band emissions in the day-side upper ionosphere and in the night-side magnetotail (Harada et al., 2019). We refer to Glassmeier and Espley (2013) for a more complete (but pre-MAVEN) review of ULF waves.

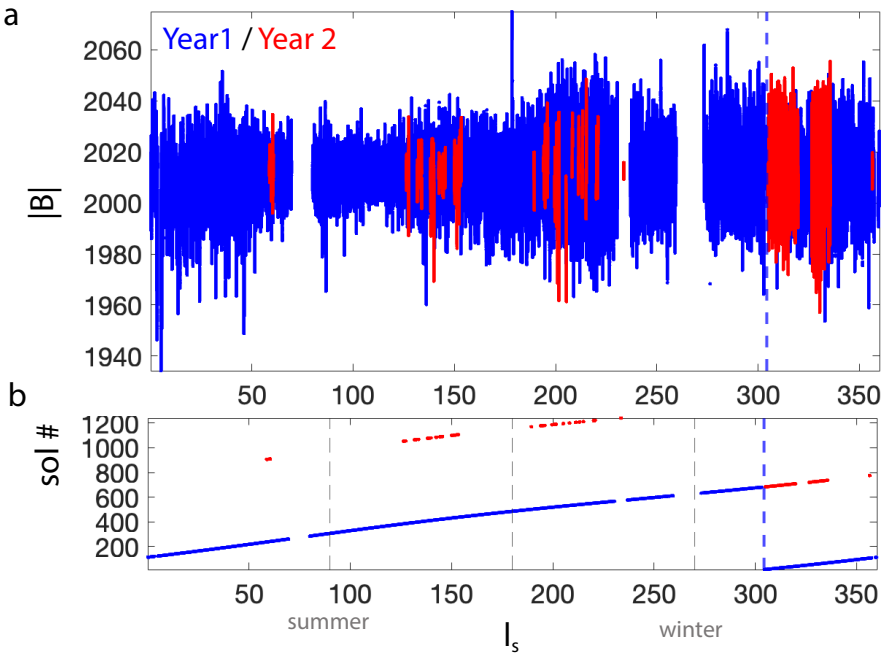

Figure 2. Magnetic field amplitude, $|B|$, measured at the InSight landing site versus solar longitude (l_s) during Martian years 1 (blue) and 2 (red) of IFG operations. All data up to sol 1241 of InSight operations are included. The blue vertical dashed line marks the beginning of the mission. (b) Corresponding InSight mission sol numbers. Vertical dashed lines indicate solstices and equinoxes.

3 Data Sets

3.1 InSight Fluxgate Magnetometer

InSight's magnetometer has been collecting data since sol 14 of the mission (Figure 2). The magnetometer operated (almost) continuously from December 11, 2018 to January 31, 2021, i.e., sols 14-736, spanning over one martian year (Figure 3). Gaps in the continuous data are mostly related to intermittent outages of the APSS data acquisition electronics and/or communication issues during solar conjunction. Subsequent, intermittent data collection resulted from power constraints due to dust accumulation on the solar panels. These later data typically span only partial sols and the last ~5 hours of data were acquired on sol 1241, on May 24, 2022. In Mars year one, 90% of all 610 sols for which data were acquired cover the full day, in year two data were acquired on 102 sols, but the IFG was operating for the full day for only 38% of those sols, and no further IFG data are currently anticipated.

We use the publicly-available, calibrated IFG data at 0.2 Hz sampling (V6 in the Planetary Data System; Russell and Joy (2020)). For intervals for which the IFG sampled at 2 Hz (sol 189 onwards), we use data down-sampled to 0.2 Hz on the ground (labelled as gpt2 on the PDS). The data is in lander level frame (Joy et al., 2019), a local frame in which the field components B_N, B_E and B_D are North, East and Down.

3.2 Satellite Magnetometer Data

MAVEN data are used for comparison with InSight observations at longer periods, specifically solar rotations. Although MAVEN measurements are available throughout

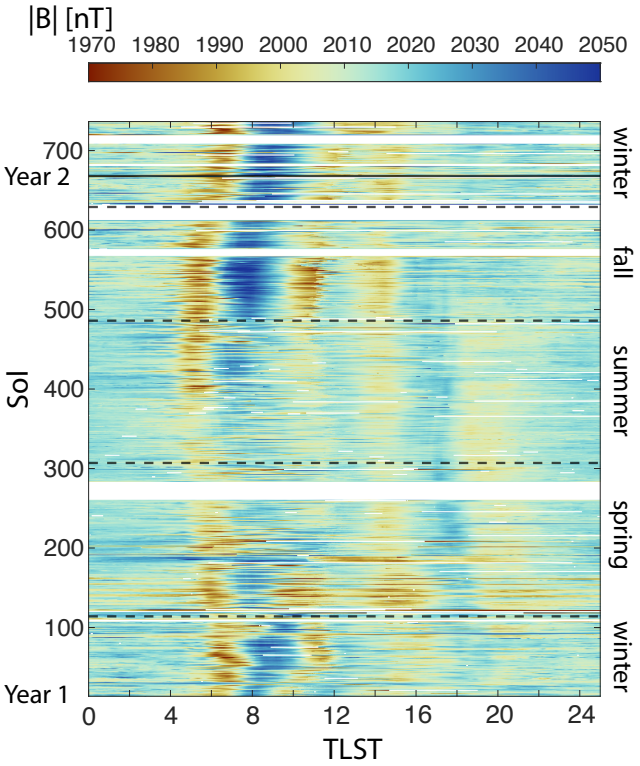

Figure 3. The magnetic field amplitude, $|B|$, versus true local solar time (TLST) for sols 14-736, the time of continous IFG operations. Data are binned in 30-second bins and the mean for each bin is shown. Dashed lines indicate solstices and equinoxes. The solid line marks sol 668 and the start of InSight's second year on Mars.

the InSight mission, the precessing orbit means that they are only occasionally acquired directly overhead the InSight landing site. Furthermore, the changing orbit geometry, means that MAVEN orbits over the InSight landing site are at differing altitudes and local times. Thus a direct comparison of individual orbital tracks with IFG data is not our focus here, but has been the subject of separate studies (Fillingim et al., 2020). Instead, here we focus on MAVEN data of the undisturbed IMF that describes solar wind activity at Mars; this allows us to investigate how changes in the IMF are seen at the surface and how much the presence of the ionosphere influences the signal. We use data in the IMF during the time of InSight operations compiled by Halekas et al. (2017), to allow e.g., joint investigations of the solar rotations (Carrington cycles) in MAVEN and IFG data. The resulting time series comprises distinct intervals during the MAVEN mission when part of MAVEN's orbit was in the solar wind. MAVEN data is shown in Mars Solar Orbit (MSO) frame in which x points from Mars towards the Sun, y points antiparallel to Mars' orbital velocity vector and z completes the right-handed system.

4 Surface Observations of Time-varying Magnetic Fields

We discuss transient and periodic external fields observed at the surface starting with a few seconds up to the longest period observable with InSight data, a Martian year (Table 1 and Figure 4). The dominant signal in the power spectral density (PSD) at the surface is the daily period and its harmonics. Shorter-period ULF waves, ranging from seconds to minutes occur intermittently and are seen in the PSD if time intervals with such occurrences are selected accordingly. The PSD falls off as $\sim$1/f for periods of a day and shorter as predicted from satellite data and used in noise models for InSight seismometer operations (Mimoun et al., 2017). Despite the data gaps, the more than one martian year of observations now constitutes several solar rotation periods, and although weak compared with the diurnal peak (Figure 4), an $\sim$26-day spectral signature is observed which is discussed further later (section 4.4). One full annual cycle allows identification of seasonal variations, although thorough analysis of seasonal and longer periodicities would require measurements for several years. In the following, we discuss InSight observations of transient and then periodic phenomena separating aspects that have been reported previously from new observations.

4.1 Previous Observations of Local Dust Movement

Dust is ubiquitous on Mars and can affect the planet globally or regionally via seasonal dust storms, but also locally via transient phenomena like dust devils in which cyclostrophic motion of triboelectrically charged dust behaves as a magnetic solenoid (Farrell, 2004; Kurgansky et al., 2007). Dust-carrying vortices, or dust devils, are common on Mars and the dust columns and/or their tracks have been captured by cameras of earlier surface and orbital missions as early as Viking (Balme & Greeley, 2006; Thomas & Gierasch, 1985).

So far InSight has not imaged any dust devils directly (Banfield et al., 2020; Lorenz et al., 2021), but orbital observations of linear tracks suggest dust devil activity at the InSight landing site (Perrin et al., 2020). Further, local dust movement identified around the InSight landing site was investigated with multiple instruments on InSight and Charalambous et al. (2021) focused on a small number of individual events for which dust transport was evident from consecutive images. Associated magnetic field changes were possibly detected, however, it was somewhat unclear if observed signals were actually driven by dust movement.

To investigate this further, Thorne et al. (2022) systematically analyzed magnetic field signals during catalogued pressure drops (Spiga et al., 2021) known to be result of passing dust devils. They found that only few events ($\sim$8%) show a significant signal at the time of pressure drops in any component. Most of the time magnetic field signals dur-

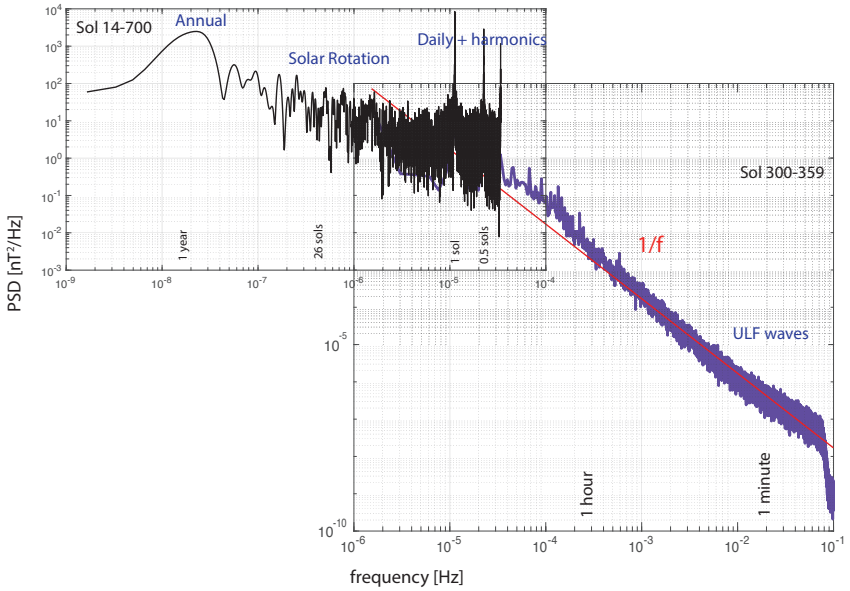

Figure 4. Power spectral density (PSD) for the surface magnetic field strength at the InSight landing site. PSD estimates for longer periods are derived using a Lomb-Scargle algorithm (black). For shorter periods (purple) a Welch spectrum was used for data from sols 300-359, a time period without large data gaps. The composite spectrum is motivated by Figure 2 in (Constable, 2007) showing an equivalent representation for the Earth.

ing a pressure drop are small, and similar to the background magnetic field. The origin of signals when observed was also investigated. Three mechanisms were explored: lander or ground tilt, solar array current generated fields, and triboelectric effects. Only the latter was found to reach observed magnitudes (>0.3 nT) in the case of exceptionally large dust devils. This is a possible explanation for the rare observations of dust devil magnetic field signatures and direct visual observations.

4.2 Space Weather

4.2.1 Previous Observations

InSight has been operating on Mars during quiet conditions of the solar cycle and little space weather has occurred so far. However, a corotating interaction region (CIR) hit Mars on December 8 and Sol 723, followed by a coronal mass ejection (CME) two sols later on December 10 and Sol 725 (Mittelholz, Johnson, Fillingim, et al., 2021). Detailed description of observations in Mittelholz, Johnson, Fillingim, et al. (2021) show the effect on the martian magnetic field at the surface and we summarize the two main findings to provide context for additional observations from 2022. First, although there was no clear onset of the CME or CIR, increased peak-to-peak (P2P) amplitudes in the diurnal variations were visible in all components, especially in the early to mid morning compared to prior sols. Magnetic field changes were seen for several days starting approximately 2 sols before the CIR peak hit and lasted until approximately 2 sols after the CME peak arrival. Second, we observed fluctuating fields with periods of tens of minutes to a few hours dominantly in the B_{East} but also in the other components during the night-time. Those mostly followed the CME.

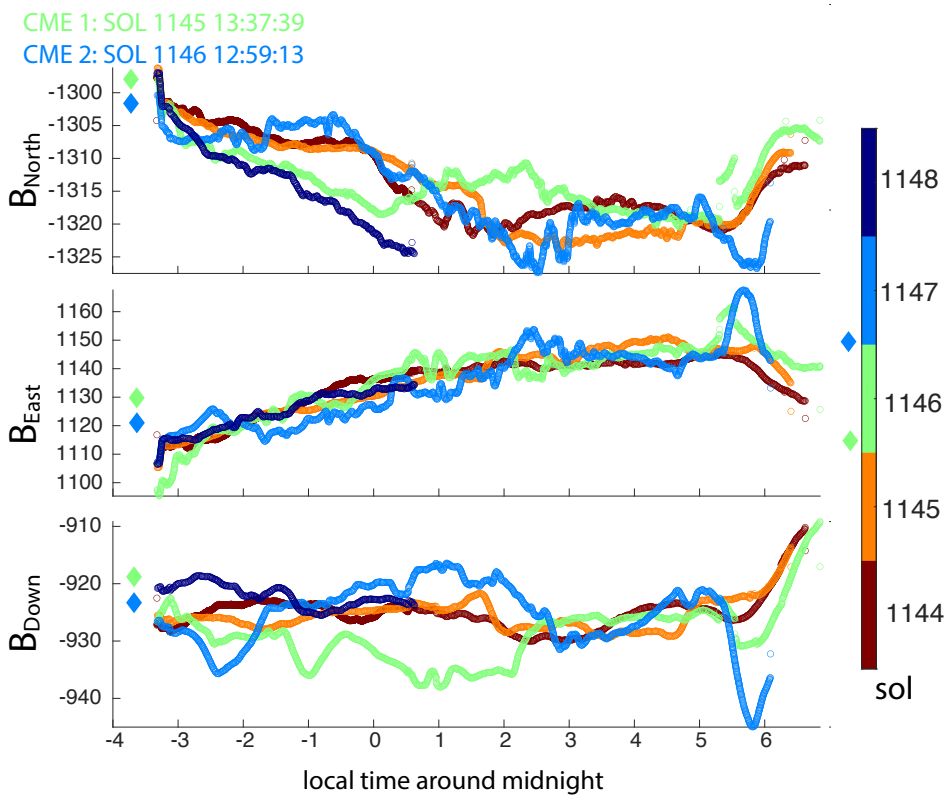

Figure 5. Effects of two CMEs from sols 1145 and 1146 (February 15-16, 2022): The 3 components of the magnetic field color coded by night. The x-axis is local time around midnight. The CMEs encountered Mars during the day on the sols marked by the colored diamonds, but there is no day-time IFG data for those sols.

4.2.2 New Observations

On February 15-16 2022, two further CMEs encountered Mars at times when the IFG was fortuitously switched on during the night-time (Figure 5). The events were weak and did not directly impact the planet, but Mars was magnetically connected to the CME flanks (see supplementary GIF). MAVEN was not in the solar wind at the time of the events, but the Solar energetic particle (SEP) instrument saw an increase in ion and electron energies. Additionally Solar Wind Ion (SWIA) and Electron Analyzer (SWEA) detect increased fluxes indicative of a compressed magnetosphere (see SFigure 1). Although the lack of day-time data does not allow investigations of the diurnal P2P signal, night-time fluctuations are again evident in the data. Although the CMEs occurred in the early afternoon on sols 1145 and 1146, we observed fluctuations on the order of 30 mins in the field lines for the following nights, similar to the events from December 2020.

In order to investigate the impact of solar wind activity on surface-based observations more generally, we made use of an orbit-averaged proxy for the upstream solar wind data for times when MAVEN is not in the solar wind (Halekas et al., 2017). We use this to investigate whether the diurnal P2P amplitude recorded by the IFG was affected by solar wind conditions as measured or inferred from the MAVEN plasma particle instrument suite. We focus on solar wind dynamic pressure, $P_{dyn} = \rho v^2$, and IMF amplitude, B, and evaluate an P_{dyn} and B per InSight sol; for sols where more than 1 orbit in the solar wind is available, we average all orbits per sol. A correlation between P_{dyn} and B is seen for MAVEN data in Figure 6a and we use those as proxy for solar wind activ-

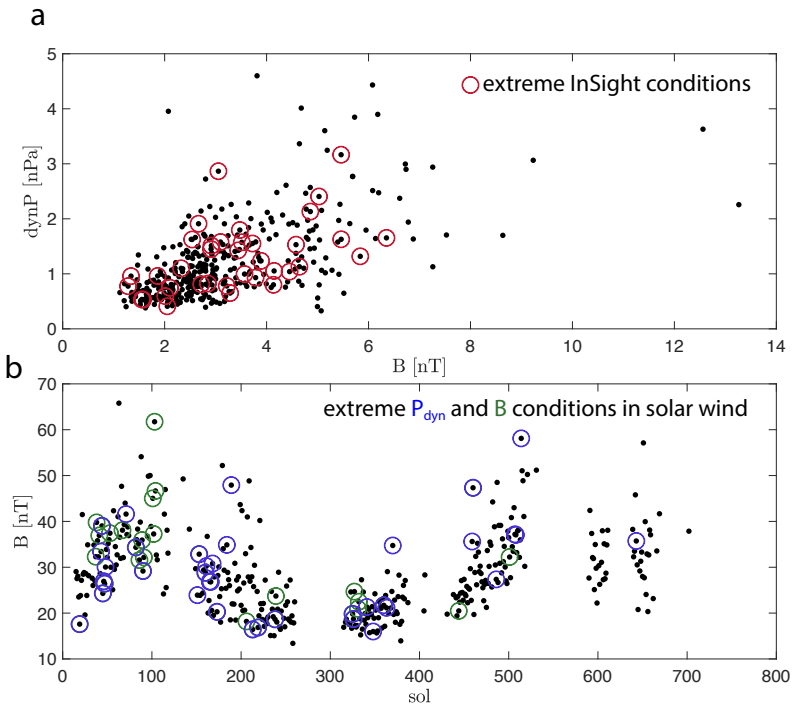

Figure 6. (a) MAVEN solar wind dynamic pressure,P_{dyn}, vs. the IMF amplitude, B, measured upstream of the bowshock. The red circles indicate days on which InSight's P2P amplitude is larger than on 90% of the sols. (b) InSight P2P amplitude versus sol. Sols with extreme (defined as highest 10%) P_{dyn} (blue) or B (green) are highlighted.

ity; however, the largest 10% of P2P amplitudes in the InSight data do not coincide with days of either proxy for high solar wind activity. Similarly, we find that InSight diurnal P2P values are uncorrelated with extreme P_{dyn} or B conditions (Figure 6b) with correlation coefficients of 0.02 and 0.03 respectively.

Overall, at least during the quiet phase of a solar cycle, magnetic signatures of solar activity at the martian surface are limited. Although during weak to moderate space weather events an increase in the diurnal P2P magnetic field amplitude is visible, it occurs gradually and the effect is not immediately obvious. An avenue of further investigation could be a focus on short period waves, which are visible during the night (Section 4.6) and thus during times at which less activity is expected from other sources such as the ionosphere or lander generated fields.

4.3 Seasonal

4.3.1 Previous Observations

We previously examined variations of the diurnal pattern for the first 389 sols on Mars and found that peak daily amplitudes vary throughout the mission and with season (Mittelholz, Johnson, Thorne, et al., 2020). Despite the incomplete annual coverage at that point, dust and seasonal variability of the atmosphere seemed to lead to variability in wind-driven ionospheric currents. Larger P2P amplitudes were found for the beginning of the mission occurring during the winter with a peak coinciding with a global dust storm, starting around sol 45 (Figure 7). We used a Mars Global Circulation Model (Forget et al., 1999; González-Galindo et al., 2013) to simulate expected ionospheric cur-

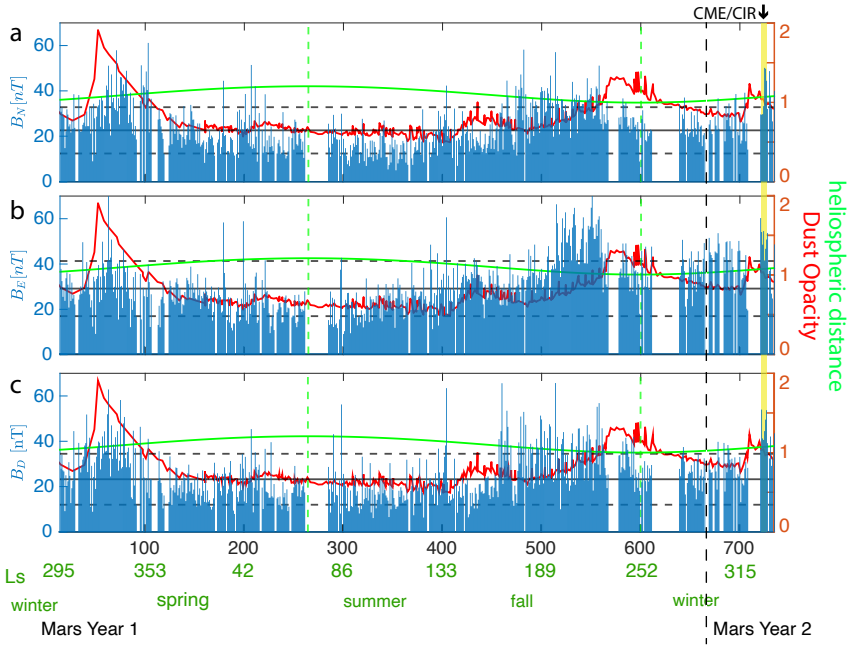

Figure 7. Peak-to-peak amplitude of B_N, B_E and B_D between 05:00 and 10:00 TLST (left y-axis) and the median (solid) value ± 1 standard deviation (dashed). Heliospheric distance in AU (green) and dust opacity (red) (right y-axis).

rents and the resulting surface magnetic fields mainly driven by predicted seasonal variations in electron density and neutral wind velocity, and assuming end-member cases for ionospheric current geometries, a line and sheet current. We estimated nominal seasonal variations in atmospheric parameters and dust storm scenarios for the dust season (Mittelholz, Johnson, Thorne, et al., 2020). The model bounds predicted by atmosphere driven fields were consistent with InSight observations. A further study decomposed magnetic field variations into their natural orthogonal components (Luo et al., 2022) and found that the first eigenmode corresponded to atmospheric variations confirming the ionosphere as primary driver of magnetic variability.

4.3.2 New observations

We perform an updated analysis of the diurnal maximum amplitudes using continuous data and MGCM predictions extending just over a full martian year, thus covering all seasons. As previously, we restrict our analysis to days for which more than 80% of the data are available and because we compare MGCM predictions for wind-driven magnetic fields Mittelholz, Johnson, Thorne, et al. (2020) with a 26-sol running mean of the maximum diurnal values, we only keep data for which the running mean includes at least 50% of the sols (13 sols). The results confirm the overall agreement between the observed and predicted field amplitudes (Figure 8). The observed magnetic field at times of dust storms (defined as times where dust opacity > 1) around sol 50-100, 540-620 and 710-725 follows the modelled predictions during dust storms well. In general, i.e. not only focused on dust storm seasons, the daily magnetic field P2P amplitude correlates with dust opacity, which further corroborates the important effect of the atmosphere on magnetic field observations (Figure 7 and 9b).

Further, we observe that diurnal peak-to-peak (P2P) variability throughout the mission is broadly anticorrelated with heliospheric distance, with lowest P2P amplitudes oc-

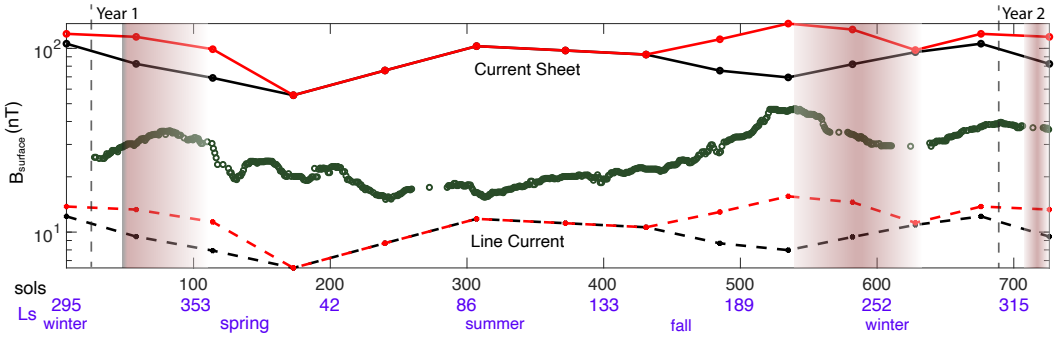

Figure 8. Wind-driven magnetic field response, $|B|$, at the surface assuming that the ionospheric dynamo current is a line current (dashed line) or a current sheet (solid line). The black line shows the prediction for an average scenario for atmospheric conditions; the red line shows the prediction for a seasonal dust storm scenario. The brown areas highlight times during which regional dust storms occurred during the InSight mission (defined as opacity larger than 1). The green curve shows the maximum amplitude of the observed magnetic field in a 26-sol running window for comparison with wind-driven predictions.

curring near aphelion or northern hemisphere summer (Figure 7 and 9a). However, the $1/r$ dependence of B seen at satellite altitudes (Mittelholz et al., 2017) is not seen on the ground.

Atmospheric parameters and IMF field strength both vary seasonally, and disentangling their effects is not fully possible. A larger ambient draped magnetic field at perihelion in the martian winter likely affects the dynamo region and enhances ionospheric fields. However, based on Figure 9 and the lack of clear correlation between solar wind parameters and the magnetic field (Section 4.2), atmospheric variations and the ionosphere seem to be the dominant drivers of the diurnal surface magnetic field variations. We conclude that currents depending on electron density, temperature and horizontal wind velocity within the ionospheric dynamo region and dust in the atmosphere are the main driver of seasonally varying P2P amplitudes in the surface magnetic field at InSight.

4.4 Carrington Rotation

4.4.1 Previous Observations

As mentioned, a study investigated sources of observed variability including the synodic Carrington period of ∼26.4 days (25.6 sols) by decomposing IFG magnetic field variations into their natural orthogonal components (Luo et al., 2022). The first eigenmode was shown to correspond to atmospheric variations, and spectral properties of the second to fifth eigenmodes resulted in a peak expected for Carrington rotations, and were thus interpreted to be driven by variations in the draped IMF.

4.4.2 New Observations

It has been challenging to observe the average synodic Carrington period in IFG data because of data gaps and the limited total duration of observations. The approximately one martian year of continuous data comprises ∼26 Carrington cycles, with multiple substantial data gaps (Figure 2). Here we use the Lomb-Scargle periodogram which is particularly suited to time series with gaps and estimates the power spectrum by directly least-square fitting to sinusoids at specified frequencies (VanderPlas, 2017).

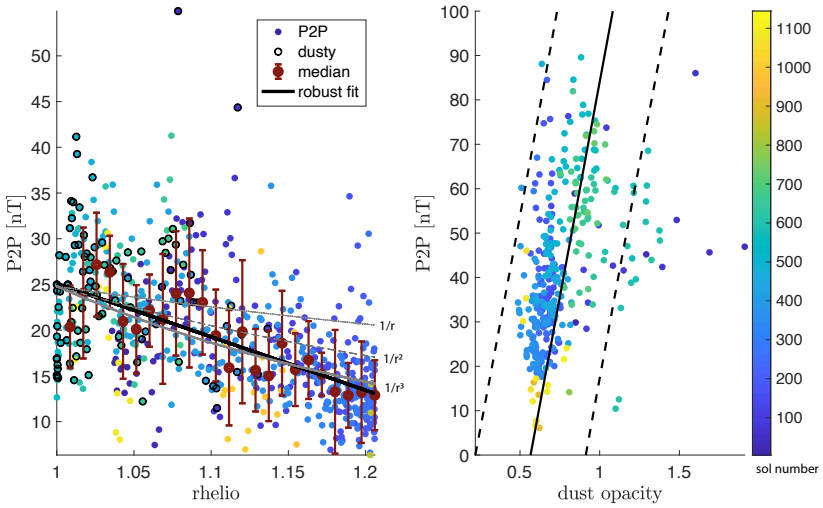

Figure 9. (a) P2P amplitudes vs. Mars distance to the Sun (normalized by minimum distance) color coded by sol number. Dark red circles and error bars represent median and standard deviation in heliospheric distance bins. Red outlined data points correspond to sols on which dust opacity is larger than 0.8. (b) P2P amplitude vs. dust opacity with a linear fit.

The Carrington period and harmonics are observed clearly in orbital data (Figure 10 a,b) during the time interval of InSight operations. MAVEN magnetic field data taken in the undisturbed solar wind (Halekas et al., 2017) show a dominant peak at 26.1 sols with additional peaks of reduced amplitude. One is at about 13 sols and likely reflects the first harmonic, the physical origin of others is unclear. The WIND spacecraft shows a spectral peak at slightly longer periods of 27 sols (note that this is given in sols for better comparison) at the same approximate time periods as MAVEN (Figure 10a). This shift is expected because of the longer synodic Carrington period at Earth c.f. Mars.

The extent to which the Carrington cycle is observed in different magnetic field components depends on the position of the planet in the Parker spiral (see Section 2). Similar power is observed in WIND data in B_x and B_y because the IMF is directed more radially outward at this heliocentric distance. In contrast, MAVEN data taken in the undisturbed IMF (Figure 10b), show little power in the B_x component, but a very dominant peak in the horizontal B_y.

We analyze InSight's spectral content in the Mars body-fixed frame (MBF) because any residual field that is static in the MBF frame will have time-varying signal in Mars Solar Orbital (MSO) frame.Two dominant peaks around 26 and 27.6 sols are observed and some other shorter period peaks, at 22 and 24.8 sols, are comparable to those observed in MAVEN data. However, different relative amplitudes for both orbital and surface data are observed. Additionally, the vertical power spectral density component (B_D) at InSight is dominant while a draped field geometry would affect horizontal components as seen in Mars orbital data. A possible reason for the dominant peak in the vertical component for IFG data is the following: The direction of currents in the ionosphere is influenced by the geometry and the strength of the background magnetic field. Gradients in the background magnetic field, e.g., from lateral variations in magnetization of the crust, lead to gradients in ionospheric (Peterson and Hall) conductivity which in turn lead to localized spatial structure in currents. At the edge of such a current system a strong vertical magnetic field component is produced. Because the IMF leads to fluctuations

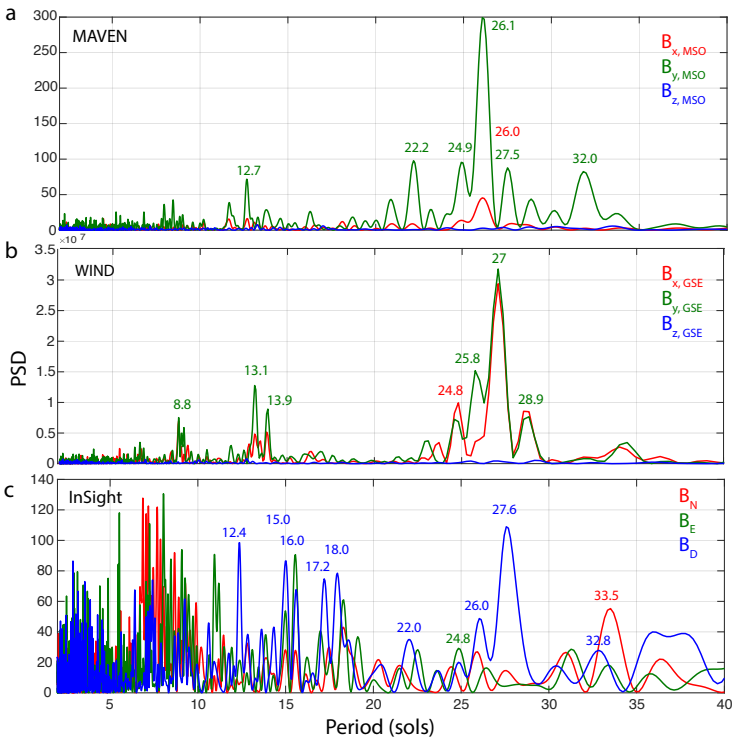

Figure 10. The power spectral density for (a) MAVEN in the undisturbed IMF at Mars (b) and WIND in the solar wind at Earth between December 2018 and October 2020. (a,b) are in the Mars Solar Orbit and Geocentric Solar Ecliptic, in both frames $\hat{X}$ points towards the Sun and $\hat{Z}$ is perpendicular to the plane of the planet's orbit around the Sun. (c) InSight data is shown in Mars Body Fixed Frame. Note that periods shorter than 2 sols are excluded. Prominent peaks are marked in colors indicating the corresponding component.

of the current system itself (Brain et al., 2003; Mittelholz et al., 2017), the contribution of this vertical magnetic field has the periodicity of the IMF. At the InSight landing site the strength of the crustal magnetic field in the dynamo region is ∼50 nT (Figure 5 in Mittelholz, Johnson, Thorne, et al. (2020)), and observed external field fluctuations are of similar magnitude (Figure 6 in Mittelholz, Johnson, Thorne, et al. (2020)). In this configuration, crustal fields that rotate below the ionosphere dynamically interact with ionospheric fields. Hence, this hypothesis implies that observations of Carrington rotations would affect different components of the magnetic field depending on strength and direction of the crustal magnetic field around the site of measurement.

4.5 Daily and Harmonics

4.5.1 Previous Observations

The diurnal variations in IFG data observed up to sol 389 have been discussed in detail (Mittelholz, Johnson, Thorne, et al., 2020). Peak amplitudes of up to 70 nT were observed and on average the largest amplitude and variability was observed in B_E and the early-to mid-morning peak.

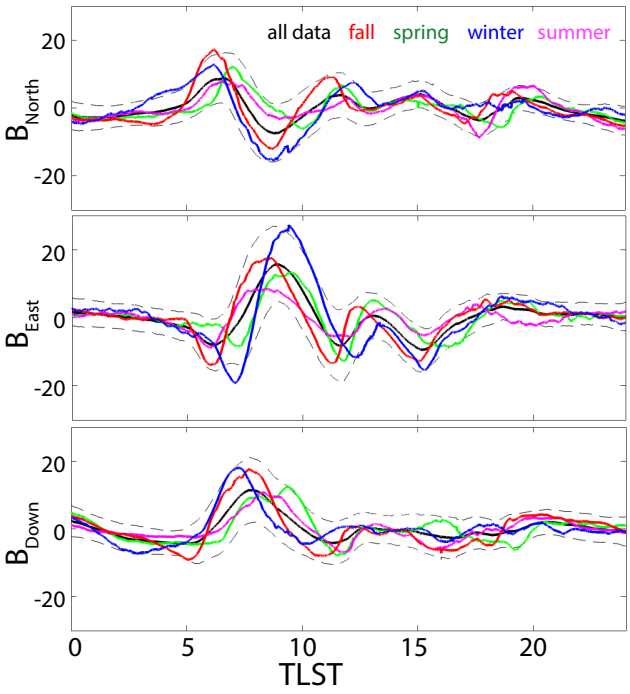

Figure 11. The 3 components of the detrended magnetic field averaged in 10000 local time bins for data within 30 degrees solar longitude of solstices and equinoxes and averaged over the all available full sol data (black) with one standard deviation uncertainty (dashed).

4.5.2 New Observations

Here we extend the analysis to include a full martian year, analyzing the 3 components of the magnetic field as a function of local time separated by season and averaged over all complete sols (Figure 11). Winter sols exhibit the largest P2P amplitude in B_{East} and the early morning. Smaller annual variability is seen during other times of the day. While summer sols show smallest P2P amplitudes (Figure 3, 7), the early morning peak still reaches the highest amplitude. As discussed before, the early morning peak coincides with times at which the product of electron density and horizontal wind velocity peaks and this effect is most pronounced during the winter; this suggests that the pattern is at least partially driven by ionospheric currents.

4.6 Short period waves

4.6.1 Previous Observations

Ultra low frequency (ULF) waves have repeatedly been observed since the first sol of IFG observations (Chi et al., 2019; Johnson et al., 2020). Known phenomena falling into this frequency range include pulsations, but also transient signals as discussed above and artificial noise, e.g., due to the solar array currents. InSight observations of pulsations with periods between seconds and minutes, likely result from the solar wind interacting with the martian magnetosphere, e.g., oscillations of the induced magnetosphere flanks or of the magnetotail (Chi et al., 2019). One example of an early ULF observation at night from sol 37 to 38 (Figure 12) shows power in the horizontal components from a few mHz to ∼50 mHz, that builds and peaks around 2 am, with virtually no power in the vertical component in this frequency band. The signal bandwidth increases as the signal amplitude increases (Figure 12a-c). Small spikes in the data (broad-band and short-

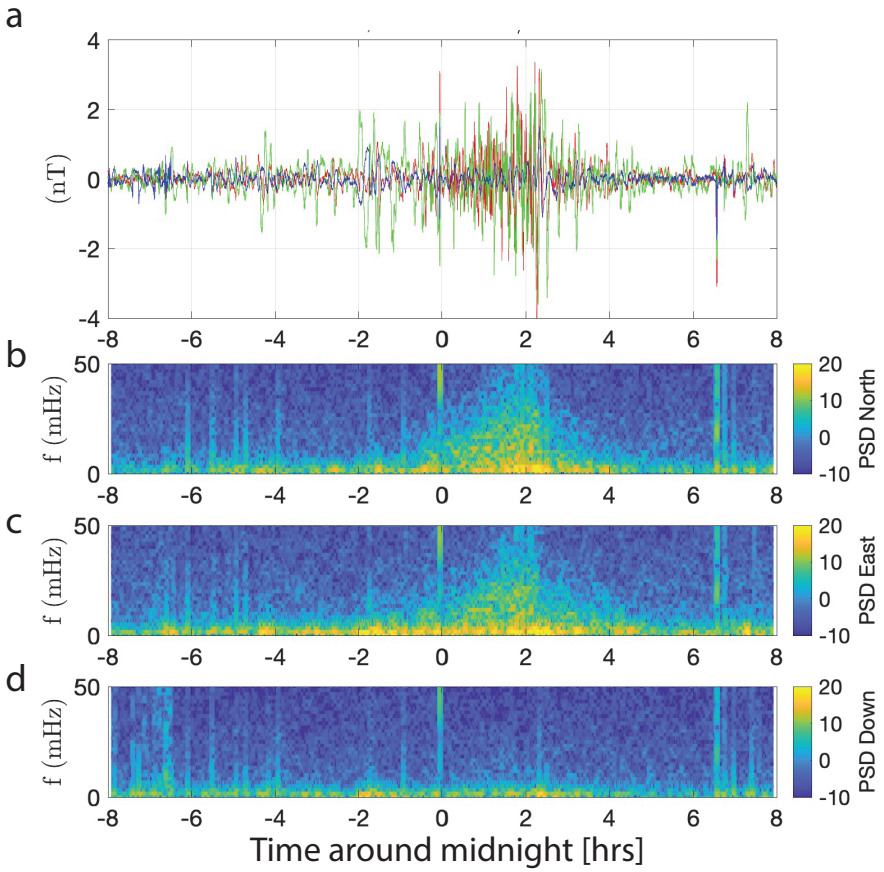

Figure 12. Wave activity on sol 37-38 / January 4-5, 2019. (a) Magnetic field components B_{North} (red), B_{East} (green) and B_{Down} (blue), detrended with a 20 minutes running mean. (b-d) Power spectral density for B_{North}, B_{East} and B_{Down}, respectively.

duration in the frequency domain), notably at midnight, are the result of lander activity.

4.6.2 New Observations

Next we focus on observations of waves in the 1-50 mHz frequency range throughout the continuous time series at the surface irrespective of their origin. Guided by the observations of individual occurrences of waves, (e.g., Figure 12), we calculate the root-mean-square (RMS) amplitude of the bandpass power in 3 frequency bands: 1 - 5 mHz, 5 - 20 mHz and 20 - 50 mHz (Figure 13). Especially, for the 1 - 5 mHz range, we observe ULF waves typically around midnight, and at dusk/dawn (Figure 12a). This occurrence is consistent with waves driven by an oscillating magnetosphere, i.e., pulsations, because during the daytime the ionosphere likely shields the lower atmosphere, preventing waves from travelling to the surface (see Figure 13a). Increased amplitudes between sunrise and sunset in all frequency bands are observed and are dominated by spacecraft contributions. The high amplitude signal before noon in the 1 - 5 mHz band is associated with the time at which solar arrays typically reach their full charge after which the solar array currents drop rapidly. Similarly to the magnetic field amplitude (Figure 3), we see substantial sol-to-sol variability and seasonal dependence. For example, in the 1 - 5 mHz

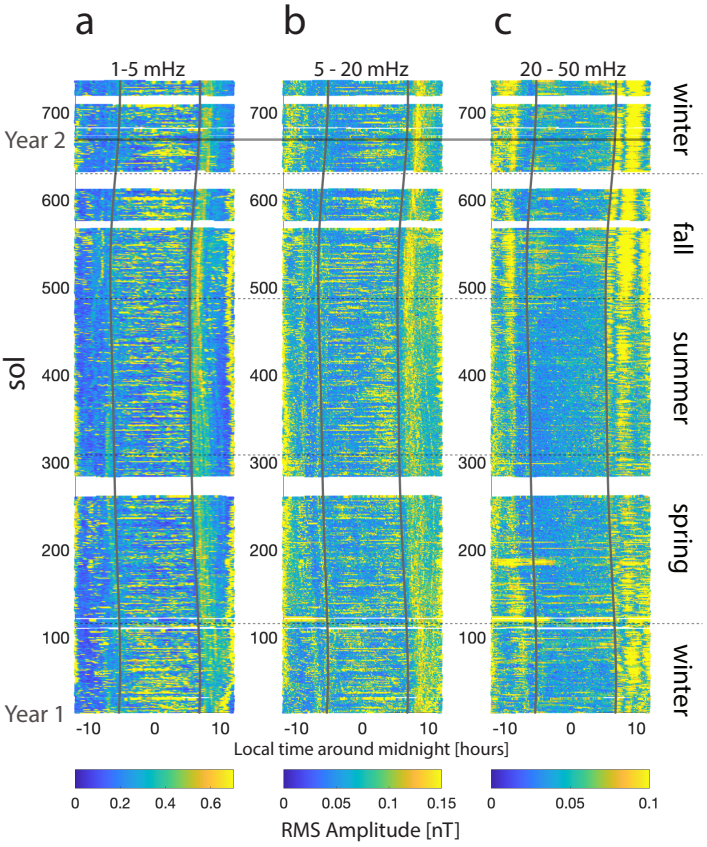

Figure 13. Bandpass power of B_{East} up to sol 732 for the frequency range of 1-5 mHz (200-1000 seconds), 5-20 mHz (50-200 seconds) and 20-50 mHz (20-50 seconds) The grey lines indicate the time of sunrise and sunset.

band, the nighttime amplitudes prior to sol 100 and after sol 500 is larger, corresponding to the northern hemisphere fall and winter. In the two higher frequency bands lander-related signals mask most natural wave activity during the day-time (see Figure 13b,c). During the night, the 5 - 20 mHz band shows similar characteristics to the 1 - 5 mHz band, but the duration of the signals is shorter, consistent with the observations in Figure 12b,c. In the highest frequency range (20 - 50 mHz), day-time noise is prevalent, and night-time RMS amplitudes are small and of short duration.

4.7 Challenges

Lastly, we point out some of the challenges that result from the lack of a dedicated cleanliness program for the IFG. In particular, we caution extensive use of the diurnal pattern and its harmonics due to difficulties in differentiating separating natural and artificial signals on diurnal time scales at the few nT level. We list important aspects that can guide further use of IFG data, but we note that the results reported here are robust with respect to these issues (Joy et al., 2019; Johnson et al., 2020; Mittelholz, Johnson, Thorne, et al., 2020; Thorne et al., 2020).

- Separation of the diurnal signal from natural and artificial sources has been discussed in (Mittelholz, Johnson, Thorne, et al., 2020; Thorne et al., 2020) in detail. Challenges are related to diurnal fluctuations in temperature and solar array currents, both of which result in peak signals during the daytime, when naturally-occurring (ionospheric or draped-IMF-related) diurnal signals are also expected to be a maximum. Calibration efforts aim to remove artificial signals (Joy et al., 2019), however, solar array currents are sampled sparsely and the temperature gain does not behave linearly.
- Further, temperature-driven effects are enhanced in the B_x component compared to B_y and B_z (Joy et al., 2019). This is of particular importance for studies in which the ratio of power in different components (e.g. vertical vs. horizontal) is evaluated (seee Section 5.1).
- Small signals such as those that might occur in association with dust devils (i.e., $<$0.5 nT), can be obscured by high frequency solar array current fluctuations. This is shown in (Thorne et al., 2022) and can bias the local times at which small naturally occurring signals can be detected.
- Although lander activity is usually easily identified (Mittelholz, Johnson, Thorne, et al., 2020), automated processing that leads to the calibrated data products on the PDS do not always fully remove such signatures, in particular those with step-like characteristics. Those artifacts affect the full band-width which complicates automatic detection of signals such as short period waves.
- Data gaps (Figure 2 and 3) throughout the mission lead to incomplete time series and challenges associated with spectral analysis. The Lomb-Scargle algorithm applied in this paper can mitigate this issue.

5 Implications

5.1 Magnetic Sounding

Time-varying magnetic fields are of particular interest for studying the interior electrical conductivity structure of a planet. Here one relies on the fact that time-varying fields induce eddy currents in the subsurface that in turn produce measurable secondary magnetic fields. The electrical conductivity can be determined from the secondary fields. Electrical conductivity is an intrinsic material property dependent on temperature and composition (Constable, 2007) and so it is complementary to other geophysical investigations.

Separation of the primary (inducing) from secondary (induced) fields to determine electrical conductivity requires information beyond data from a single magnetometer. In classical geomagnetic sounding (e.g, (Banks, 1969)), the primary field geometry is assumed to be a dipole formed from Earth's ring current (which in turn is manifested from the strong intrinsic dipole field). Signals spanning many decades in frequency are all constrained by the same simple geometry. The theory relates the vertical field to the horizontal gradients of the horizontal fields through a frequency-dependent inductive length scale or penetration depth that varies with electrical conductivity (Olsen, 1999). Because the gradients are computed analytically, the ratios of vertical to horizontal fields can be used directly, hence this method is also called the Z/H technique. Similarly, Mittelholz, Grayver, et al. (2021) estimated the electrical conductivity of the Moon assuming that the source field in Earth's magnetotail followed a dipole.

In spite of a strong degree-one (day-night) signal in Mars' ionospheric variation, attempts at geomagnetic sounding have not been successful. Multipole analysis has been similarly inhibited, although comparable efforts using Earth's solar-quiet (Sq) ionospheric variations have enjoyed limited success (Bahr & Filloux, 1989). The geometry of ionospheric variations on Mars have been studied using satellites (Section 2), but their spatial structure is still complex and not easily explained by a simple geometry, i.e. only

a specific subset of Gauss coefficients. Specifically for InSight data, several challenges have become apparent to derive electrical conductivity (Mittelholz, Johnson, Grimm, et al., 2020). First, the relationships between vertical and horizontal components do not follow poloidal-induction theory and further diurnal signals in particular remain suspect because of contamination from spacecraft fields (see section 4.7).

Additional measurements could circumvent the dependency on assumed geometry and resolve these issues. Horizontal field gradients can be directly estimated using a magnetometer array (Gough & Ingham, 1983). This was the approach proposed for Netlander (Pinçon et al., 2000). The magnetic transfer function between orbiting and landed spacecraft was used successfully for the Moon (Sonett (1982) for a review) but Mars' intervening ionosphere appears to reduce coherence. Alternatively, the magnetotelluric method (e.g., Vozoff (1991)) measures the time-varying electric field at the surface in addition to the magnetic field. This is a complete single-station sounding that only weakly depends on source geometry (R. E. Grimm & Delory, 2012) and is currently in development for planetary missions (R. Grimm et al., 2021).

5.2 Future Observations

InSight's magnetometer has enabled a range of observations of time-varying magnetic fields at the landing site, over a time frame of more than one martian year. Including magnetometers on future missions at a variety of locations and thus extending the spatial distribution and time span of such observations will be of great value in understanding a range of phenomena:

1. Above we discuss the crustal magnetic field interacting with the IMF and ionospheric currents. While the above discussion is motivated by InSight results and thus a unique crustal magnetic field setting, the influence of crustal magnetization on the ionosphere could be tested under different field geometries and amplitudes.
   For example, for the spectral content at the 26-sol period, we suggest that power partitioning among the different field components at InSight results from the crustal magnetic field geometry interacting with the ionosphere (section 4.4). Following the same argument, we predict that at a different landing site, with weaker or no crustal fields affecting ionospheric currents, a diurnal signal in mainly the horizontal components would be expected. Large-scale strong magnetic fields above the instrument (as observed in regions such as Terra Cimmeria / Sirenum) would likely also lead to a horizontally dominant peak reflecting compression and extension of closed crustal fields due to varying magnetic pressure.
   Further, the geometry of the crustal magnetic field at the landing site influences local ionospheric conductivity and the dynamo region directly. A different background field would thus lead to a different magnetic field environment (Lillis et al., 2019; Fillingim et al., 2012).
2. At other mission landing sites such as those of Spirit, Curiosity or Perseverance, multiple dust devil images provide evidence for dust being lofted while this observation has not been made with InSight. It is thus not clear if the paucity of magnetic field signals at the times of pressure vortices simply reflects a lack of dusty vortices. If there was dust lofted more readily, could we frequently observe signals associated with pressure drops?
3. The solar cycle is currently in its ascending phase and will peak in 2026, while the IFG has been operating during a quiet period. A longer time series covering a full solar cycle, especially during solar maximum, increases the probability of observing large space weather events. Measuring the magnetic field response of such events at multiple sites would be particularly useful, especially if such observations were also made simultaneously by orbital spacecraft. In orbit, crustal field topology is

589 known to be affected by CMEs where in weak/strong crustal fields an increase in
590 draped/open field lines is observed (Xu et al., 2019; Luhmann et al., 2017). Open
591 crustal field lines can reconnect with solar wind field lines in a process called re-
592 connection, leading to a direct connection of plasma environment to the surface.
593 Direct access to the lower atmosphere and surface, leads to increased atmospheric
594 escape (Xu et al., 2019; Luhmann et al., 2017) and radiation doses as shown by
595 the radiation experiment on Mars Science Laboratory (Hassler et al., 2012). An
596 additional instrument suite describing the plasma environment would further en-
597 hance understanding of space weather effects at the surface, an important aspect
598 for future human exploration efforts.
599 4. The limited duration of the IFG time series does not allow robust characteriza-
600 tion of annual variability and long term trends. Installation of long-time obser-
601 vatories on the surface of Mars would allow long-term tracking of magnetic vari-
602 ability on Mars and better statistics on space weather events, as available on Earth.

603 6 Conclusion

604 InSight has offered us the first observations of time-varying magnetic fields as seen
605 from the surface. We summarize observations ranging from periods of minutes to a year,
606 and transient signals using data acquired during the entire mission, but focused on the
607 first martian year. Transients include signals associated with local dust movement and
608 space weather, periodic signals include ultra low frequency waves, diurnal signals, Car-
609 rington rotations and seasonal variations. Major drivers of time-varying magnetic fields
610 are ionospheric currents and direct solar wind interactions appear to be a secondary ef-
611 fect. In particularly the effect of dust storms and seasonal variations on diurnal and shorter
612 periods, and the overall correlation of peak diurnal amplitudes with dust opacity (Fig-
613 ure 9) strengthens this hypothesis. Although the direct impact of the solar wind dur-
614 ing space weather can be observed, producing peak diurnal amplitudes that are compa-
615 rable to those at the times of dust storms (Fig 7), there is not direct correlation between
616 solar wind activity and surface magnetic field observations. At the 26-sol period, the power
617 in the vertical B_{Down} dominates, rather than the horizontal components that would be
618 indicative of the draped IMF. This further corroborates an indirect effect of the IMF,
619 i.e., the IMF likely affects the ionosphere leading to current systems which are ultimately
620 observed on the ground.

621 The crustal magnetic field environment affects the geometry and amplitude of iono-
622 spheric currents and observations of resulting magnetic fields are thus dependent on crustal
623 magnetization at the landing site. Future magnetic field data acquisition at a variety of
624 landing sites will thus shed further light on Mars' dynamic environment. The upcom-
625 ing Exomars mission and its magnetometers will land in a rather strongly magnetized
626 region and will provide a different perspective on crustal field line interaction with ex-
627 ternal field fluctuations. China's Zhurong rover's lading site is in a region of weaker crustal
628 field strength c.f. InSight (Langlais et al., 2019), potentially allowing investigations of
629 some of the open issues raised above. This will allow studying the local nature and de-
630 pendency on individual sites to the propagation of signals to the surface. Future explo-
631 ration with low altitude platforms such as balloons or helicopters will open up even fur-
632 ther possibilities in exploring multiple landing sites on a regional scale (Mittelholz et al.,
633 2022; Bapst et al., 2021; Hall et al., 2007).

634 Acknowledgments

635 We acknowledge NASA, CNES, their partner agencies and Institutions (UKSA, SSO,
636 DLR, JPL, IPGP-CNRS, ETHZ, IC, MPS-MPG) and flight operations team at JPL, SIS-
637 MOC (SEIS on Mars Operations Center) and MSDS (Mars SEIS Data Service). We ac-
638 knowledge support from Harvard's Daly Postdoctoral Fellowship (A.M.), the Natural Sci-

ences and Engineering Research Council of Canada (S.T., C.L.J) and the InSight Mission (C.L.J, S.J., M.F., S.S., W.B.). This research was carried out in part at the Jet Propulsion Laboratory, California Institute of Technology, under a contract with the National Aeronautics and Space Administration (80NM0018D0004).This paper is InSight Contribution Number 222.

Open Research

All InSight data used in this study is publicly available via the Planetary Data System at `https://doi.org/10.17189/1519202`. Data from the MAVEN mission are available via the Planetary Data System at `https://pds-ppi.igpp.ucla.edu/search/view/?f=yes&id=pds://PPI/maven.mag.calibrated/data`. Upstream and proxy solar wind data (Halekas et al., 2017) can be accessed at `http://www.physics.uiowa.edu/~jhalekas/drivers.html`.

References

A Mittelholz, Johnson, C., Thorne, S., Chi, P., Fillingim, M., Joy, S., ... Banerdt, W. (2022). The External Magnetic Field as Seen from InSight. *LPI Contributions*, *2678*, 1242.

Acuna, M. H., Connerney, J. E. P., Ness, N. F., Lin, R. P., Mitchell, D., Carlson, C. W., ... Cloutier, P. (1999). Global Distribution of Crustal Magnetization Discovered by the Mars Global Surveyor MAG/ER Experiment. *Science*, *284*(5415), 790–793. doi: 10.1126/science.284.5415.790

Bahr, K., & Filloux, J. H. (1989). Local Sq response functions from EMSLAB data. *Journal of Geophysical Research: Solid Earth*, *94*(B10), 14195–14200. Retrieved from https://agupubs.onlinelibrary.wiley.com/doi/abs/10.1029/JB094iB10p14195 doi: https://doi.org/10.1029/JB094iB10p14195

Balme, M., & Greeley, R. (2006). Dust devils on Earth and Mars. *Reviews of Geophysics*, *44*(3). Retrieved from https://agupubs.onlinelibrary.wiley.com/doi/abs/10.1029/2005RG000188 doi: https://doi.org/10.1029/2005RG000188

Banerdt, W. B., Smrekar, S., Banfield, D., Giardini, D., Golombek, M. P., Johnson, C., ... Wieczoreck, M. (2020). Initial Results from the InSight Mission on Mars. *Nature Geoscience*, *13*(March), 183–189. Retrieved from http://dx.doi.org/10.1038/s41561-020-0544-y doi: 10.1038/s41561-020-0544-y

Banfield, D., Rodriguez-Manfredi, J. A., Russell, C. T., Rowe, K. M., Leneman, D., Lai, H. R., ... Team, T. T. (2018). InSight Auxiliary Payload Sensor Suite (APSS). *Space Science Reviews*, *215*(1), 4. Retrieved from https://doi.org/10.1007/s11214-018-0570-x doi: 10.1007/s11214-018-0570-x

Banfield, D., Spiga, A., Newman, C., Forget, F., Lemmon, M., Lorenz, R., ... Banerdt, W. B. (2020). The atmosphere of Mars as observed by InSight. *Nature Geoscience*, *13*(March). Retrieved from http://www.nature.com/articles/s41561-020-0534-0 doi: 10.1038/s41561-020-0534-0

Banks, R. J. (1969). Geomagnetic Variations and the Electrical Conductivity of the Upper Mantle. *Geophysical Journal International*, *17*(5), 457–487. Retrieved from https://doi.org/10.1111/j.1365-246X.1969.tb00252.x doi: 10.1111/j.1365-246X.1969.tb00252.x

Bapst, J., Parker, T. J., Balaram, J., Tzanetos, T., Matthies, L. H., Edwards, C. D., ... Weiss, B. P. (2021). Mars Science Helicopter: Compelling Science Enabled by an Aerial Platform. *Bulletin of the AAS*, *53*(4). Retrieved from https://baas.aas.org/pub/2021n4i361 doi: 10.3847/25c2cfeb.a126aea0

Brain, D., Bagenal, F., Acuña, M. H., & Connerney, J. (2003). Martian magnetic morphology: Contributions from the solar wind and crust. *Journal of Geophysical Research*, *108*(A12), 1424. Retrieved from http://dx.doi.org/10.1029/2002JA009482{\%}5CnUsers/wang/GoogleDrive/Papers/brain2003.pdf doi: 10.1029/2002JA009482

Brain, D., Bagenal, F., Acuña, M. H., Connerney, J. E., Crider, D. H., Mazelle, C., ... Ness, N. F. (2002). Observations of low-frequency electromagnetic plasma waves upstream from the Martian shock. *Journal of Geophysical Research: Space Physics*, *107*(A6). doi: 10.1029/2000JA000416

Brain, D., Mitchell, D. L., & Halekas, J. S. (2006). The magnetic field draping direction at Mars from April 1999 through August 2004. *Icarus*, *182*(2), 464–473. Retrieved from http://www.sciencedirect.com/science/article/pii/S0019103505004902{\%}5CnUsers/wang/GoogleDrive/Papers/brain2006a.pdf doi: 10.1016/j.icarus.2005.09.023

Charalambous, C., McClean, J. B., Baker, M., Pike, W. T., Golombek, M., Lemmon, M., ... Banerdt, W. B. (2021). Vortex-Dominated Aeolian Activity at InSight's Landing Site, Part 1: Multi-Instrument Observations, Analysis, and Implications. *Journal of Geophysical Research: Planets*, *126*(6), 1–51. doi: 10.1029/2020je006757

Chi, P., Russell, C., Yu, Y., Joy, S., Ma, Y., Banfield, D., ... Banerdt, W. (2019, dec). InSight Observations of Magnetic Pulsations on Martian Surface: Morphology and Wave Sources. In *Agu fall meeting abstracts* (Vol. 2019, pp. DI51B—-0024).

Connerney, J. E. P., Espley, J. R., Dibraccio, G. A., Gruesbeck, J. R., Oliversen, R. J., Mitchell, D. L., ... Jakosky, B. M. (2015). First results of the MAVEN magnetic field investigation. *Geophysical Research Letters*, *42*, 8819– 8827. doi: 10.1002/2015GL065366

Constable, S. (2007). Geomagnetic induction studies. *Geomagnetism*, 237–276. Retrieved from `http://ci.nii.ac.jp/naid/10030366661/en/`

Crider, D., Vignes, D., Krymskii, A. M., Breus, T., Ness, N. F., Mitchell, D. L., ... Acuña, M. H. (2003). A proxy for determining solar wind dynamic pressure at Mars using Mars Global Surveyor data. *Journal of Geophysical Research*, *108*(A12), 1461. Retrieved from `http://dx.doi.org/10.1029/2003JA009875{\%}5CnUsers/wang/GoogleDrive/Papers/2003JA009875.pdf` doi: 10.1029/2003JA009875

Espley, J. R., Cloutier, P. A., Brain, D. A., Crider, D. H., & Acuña, M. H. (2004). Observations of low-frequency magnetic oscillations in the Martian magnetosheath, magnetic pileup region, and tail. *Journal of Geophysical Research: Space Physics*, *109*(A7). doi: 10.1029/2003JA010193

Espley, J. R., Cloutier, P. A., Crider, D. H., Brain, D. A., & Acuña, M. H. (2005). Low-frequency plasma oscillations at Mars during the October 2003 solar storm. *Journal of Geophysical Research: Space Physics*, *110*(A9). Retrieved from `https://agupubs.onlinelibrary.wiley.com/doi/abs/10.1029/2004JA010935` doi: https://doi.org/10.1029/2004JA010935

Espley, J. R., Delory, G. T., & Cloutier, P. A. (2006). Initial observations of low-frequency magnetic fluctuations in the Martian ionosphere. *Journal of Geophysical Research E: Planets*, *111*(6), 1–7. doi: 10.1029/2005JE002587

Farrell, W. M. (2004). Electric and magnetic signatures of dust devils from the 2000–2001 MATADOR desert tests. *Journal of Geophysical Research*, *109*(E3), 1–13. doi: 10.1029/2003je002088

Felici, M., Withers, P., Smith, M. D., González-Galindo, F., Oudrhiri, K., & Kahan, D. (2020). MAVEN ROSE Observations of the Response of the Martian Ionosphere to Dust Storms. *Journal of Geophysical Research: Space Physics*, *125*(6), 1–17. doi: 10.1029/2019JA027083

Ferguson, B. B., Cain, J. C., Crider, D. H., Brain, D. a., & Harnett, E. M. (2005). External fields on the nightside of Mars at Mars Global Surveyor mapping altitudes. *Geophysical Research Letters*, *32*(16), 1–4. doi: 10.1029/2004GL021964

Fillingim, M. O., Johnson, C. L., Mittelholz, A. M., Langlais, B., Russell, C. T., Joy, S. P. P., ... al., E. (2020). A first comparison between ionospheric and surface level magnetic fields at Mars. *Earth and Space Science Open Archive*, 14. Retrieved from `https://doi.org/10.1002/essoar.10503286.1` doi: 10.1002/essoar.10503286.1

Fillingim, M. O., Lillis, R. J., England, S. L., Peticolas, L. M., Brain, D. A., Halekas, J. S., ... Bougher, S. W. (2012). On wind-driven electrojets at magnetic cusps in the nightside ionosphere of Mars. *Earth, Planets and Space*, *64*(2), 93–103. doi: 10.5047/eps.2011.04.010

Fillingim, M. O., Peticolas, L. M., Lillis, R. J., Brain, D. A., Halekas, J. S., Lummerzheim, D., & Bougher, S. W. (2010). Localized ionization patches in the nighttime ionosphere of Mars and their electrodynamic consequences. *Icarus*, *206*(1), 112–119. Retrieved from `http://dx.doi.org/10.1016/j.icarus.2009.03.005` doi: 10.1016/j.icarus.2009.03.005

Forget, F., Hourdin, F., Fournier, R., Hourdin, C., Talagrand, O., Collins, M., ... Huot, J. P. (1999). Improved general circulation models of the Martian at-

mosphere from the surface to above 80 km. *Journal of Geophysical Research: Planets*, *104*(E10), 24155–24175. doi: 10.1029/1999JE001025

Glassmeier, K. H., & Espley, J. (2013). ULF Waves in Planetary Magnetospheres. *Magnetospheric ULF Waves: Synthesis and New Directions*, *169*(d), 341–359. doi: 10.1029/169GM22

González-Galindo, F., Chaufray, J.-Y., López-Valverde, M. A., Gilli, G., Forget, F., Leblanc, F., ... Yagi, M. (2013). Three-dimensional Martian ionosphere model: I. The photochemical ionosphere below 180 km. *Journal of Geophysical Research: Planets*, *118*(10), 2105–2123. Retrieved from https://agupubs.onlinelibrary.wiley.com/doi/abs/10.1002/jgre.20150 doi: 10.1002/jgre.20150

Gough, D. I., & Ingham, M. R. (1983). Interpretation methods for magnetometer arrays. *Reviews of Geophysics*, *21*(4), 805–827. Retrieved from https://agupubs.onlinelibrary.wiley.com/doi/abs/10.1029/RG021i004p00805 doi: https://doi.org/10.1029/RG021i004p00805

Grimm, R., Nguyen, T., Persyn, S., Phillips, M., Stillman, D., Taylor, T., ... Sheppard, D. (2021). A magnetotelluric instrument for probing the interiors of Europa and other worlds. *Advances in Space Research*, *68*(4), 2022–2037. Retrieved from https://www.sciencedirect.com/science/article/pii/S0273117721002969 doi: https://doi.org/10.1016/j.asr.2021.04.011

Grimm, R. E., & Delory, G. T. (2012). Next-generation electromagnetic sounding of the Moon. *Advances in Space Research*, *50*(12), 1687–1701. Retrieved from http://dx.doi.org/10.1016/j.asr.2011.12.014 doi: 10.1016/j.asr.2011.12.014

Halekas, J. S., Ruhunusiri, S., Harada, Y., Collinson, G., Mitchell, D. L., Mazelle, C., ... Jakosky, B. M. (2017). Structure, dynamics, and seasonal variability of the Mars-solar wind interaction: MAVEN Solar Wind Ion Analyzer in-flight performance and science results. *Journal of Geophysical Research: Space Physics*, *122*(1), 547–578. doi: 10.1002/2016JA023167

Hall, J. L., Pauken, M. T., Kerzhanovich, V. V., Walsh, G. J., Fairbrother, D., Shreves, C., & Lachenmeier, T. (2007). Flight test results for aerially deployed mars balloons. *AIAA Balloon Systems Conference, 2007*, 262–274.

Harada, Y., Ruhunusiri, S., Halekas, J. S., Espley, J., DiBraccio, G. A., Mcfadden, J. P., ... Jakosky, B. M. (2019). Locally Generated ULF Waves in the Martian Magnetosphere: MAVEN Observations. *Journal of Geophysical Research: Space Physics*, *124*(11), 8707–8726. doi: 10.1029/2019JA027312

Hassler, D. M., Zeitlin, C., Wimmer-Schweingruber, R. F., Böttcher, S., Martin, C., Andrews, J., ... Cucinotta, F. A. (2012). The Radiation Assessment Detector (RAD) investigation. *Space Science Reviews*, *170*(1-4), 503–558. doi: 10.1007/s11214-012-9913-1

Jakosky, B. M., Lin, R. P., Grebowsky, J. M., Luhmann, J. G., Mitchell, D. F., Beutelschies, G., ... Zurek, R. (2015). The Mars Atmosphere and Volatile Evolution (MAVEN) Mission. *Space Science Reviews*, 3–48. Retrieved from http://dx.doi.org/10.1007/s11214-015-0139-x doi: 10.1007/s11214-015-0139-x

Johnson, C. L., Mittelholz, A., Langlais, B., Russell, C. T., Ansan, V., Banfield, D., ... Banerdt, W. B. (2020). Crustal and time-varying magnetic fields at the InSight landing site on Mars. *Nature Geoscience*, *13*(3), 199–204. Retrieved from http://dx.doi.org/10.1038/s41561-020-0537-x doi: 10.1038/s41561-020-0537-x

Joy, S. P., Mafi, J. N., & Slavney, S. (2019). Interior Exploration Using Seismic Investigations, Geodesy, and Heat Transport (InSight) Mission Insight Fluxgate Magnetometer (IFG) PDS Archive Software Interface Specification. doi: https://doi.org/10.17189/1519206

Knapmeyer-Endrun, B., Panning, M. P., Bissig, F., Joshi, R., Khan, A., Kim, D., ... Banerdt, W. B. (2021). Thickness and structure of the martian crust from InSight seismic data. *Science*, *373*(6553), 438–443. doi: 10.1126/science.abf8966

Kurgansky, M. V., Baez, L., & Ovalle, E. M. (2007). A simple model of the magnetic emission from a dust devil. *Journal of Geophysical Research E: Planets*, *112*(11), 1–7. doi: 10.1029/2007JE002952

Langlais, B., Thébault, E., Houliez, A., Purucker, M. E., & Lillis, R. J. (2019). A New Model of the Crustal Magnetic Field of Mars Using MGS and MAVEN. *Journal of Geophysical Research: Planets*, *124*(6), 1542–1569. doi: 10.1029/2018JE005854

Lee, C. O., Hara, T., Halekas, J. S., Thiemann, E., Chamberlin, P., Eparvier, F., ... Jakosky, B. M. (2017). MAVEN observations of the solar cycle 24 space weather conditions at Mars. *Journal of Geophysical Research: Space Physics*, *122*(3), 2768–2794. doi: 10.1002/2016JA023495

Lee, C. O., Jakosky, B. M., Luhmann, J. G., Brain, D. A., Mays, M. L., Hassler, D. M., ... Halekas, J. S. (2018). Observations and Impacts of the 10 September 2017 Solar Events at Mars: An Overview and Synthesis of the Initial Results. *Geophysical Research Letters*, *45*(17), 8871–8885. doi: 10.1029/2018GL079162

Lillis, R. J., Fillingim, M. O., Ma, Y., Gonzalez-Galindo, F., Forget, F., Johnson, C. L., ... Fowler, C. M. (2019). Modeling Wind-Driven Ionospheric Dynamo Currents at Mars: Expectations for InSight Magnetic Field Measurements. *Geophysical Research Letters*, *46*(10), 5083–5091. doi: 10.1029/2019GL082536

Lillis, R. J., Robbins, S., Manga, M., Halekas, J. S., & Frey, H. V. (2013). Time history of the Martian dynamo from crater magnetic field analysis. *Journal of Geophysical Research E: Planets*, *118*(7), 1488–1511. doi: 10.1002/jgre.20105

Lorenz, R. D., Lemmon, M. T., & Maki, J. (2021). First Mars year of observations with the InSight solar arrays: Winds, dust devil shadows, and dust accumulation. *Icarus*, *364*, 114468. Retrieved from `https://www.sciencedirect.com/science/article/pii/S0019103521001494` doi: https://doi.org/10.1016/j.icarus.2021.114468

Luhmann, J. G., Dong, C. F., Ma, Y. J., Curry, S. M., Xu, S., Lee, C. O., ... Jakosky, B. M. (2017). Martian magnetic storms. *Journal of Geophysical Research: Space Physics*, *122*(6), 6185–6209. doi: 10.1002/2016JA023513

Luo, H., Du, A. M., Ge, Y. S., Johnson, C. L., Mittelholz, A., Zhang, Y., ... Xu, W. Y. (2022). Natural Orthogonal Component Analysis of Daily Magnetic Variations at the Martian Surface: InSight Observations. *Journal of Geophysical Research: Planets*, *127*(2), 1–15. doi: 10.1029/2021JE007112

Mimoun, D., Murdoch, N., Lognonné, P., Hurst, K., Pike, W. T., Hurley, J., ... Banerdt, W. B. (2017). The Noise Model of the SEIS Seismometer of the InSight Mission to Mars. *Space Science Reviews*, *211*(1-4), 383–428. Retrieved from `http://dx.doi.org/10.1007/s11214-017-0409-x` doi: 10.1007/s11214-017-0409-x

Mitteholz, A., & Johnson, C. L. (2022). The Martian Crustal Magnetic Field. *Frontiers in Astronomy and Space Sciences*, *9*(895362). doi: 10.3389/fspas.2022.895362

Mittelholz, A., Grayver, A., Khan, A., & Kuvshinov, A. (2021). The Global Conductivity Structure of the Lunar Upper and Mid Mantle. *Journal of Geophysical Research: Planets*, *126*(111), e2021JE006980. Retrieved from `https://agupubs.onlinelibrary.wiley.com/doi/abs/10.1029/2021JE006980` doi: https://doi.org/10.1029/2021JE006980

Mittelholz, A., Heagy, L., Johnson, C. L., Langlais, B., Lillis, R. J., & Rapin, W. (2022). Helicopter Magnetic Field Surveys for Future Mars Missions. *LPI Contributions*, *2655*, 5016.

Mittelholz, A., Johnson, C., Grimm, R., Haviland, H., Langlais, B., Lognonné, P., ... Banerdt, W. (2020, dec). Towards magnetic sounding of Mars using diurnal variations. In *Agu fall meeting abstracts* (Vol. 2020, pp. DI026–03).

Mittelholz, A., Johnson, C. L., Feinberg, J. M., Langlais, B., & Phillips, R. J. (2020). Timing of the martian dynamo : New constraints for a core field 4 . 5 and 3 . 7 Ga ago. *Science Advances*, *18*(May), 1–8. doi: 10.1126/sciadv.aba0513

Mittelholz, A., Johnson, C. L., Fillingim, M., Joy, S., Espley, J. R., Halekas, J., ... Banerdt, W. (2021). Space Weather Observations with InSight. *Geophysical Research Letters*.

Mittelholz, A., Johnson, C. L., & Lillis, R. J. (2017). Global-scale External Magnetic Fields at Mars Measured at Satellite Altitude. *Journal of Geophysical Research: Planets*, *112*, 1243–1257. Retrieved from `http://doi.wiley.com/10.1002/2017JE005308` doi: 10.1002/2017JE005308

Mittelholz, A., Johnson, C. L., & Morschhauser, A. (2018). A New Magnetic Field Activity Proxy for Mars From MAVEN Data. *Geophysical Research Letters*, *45*(12), 5899–5907. Retrieved from `https://agupubs.onlinelibrary.wiley.com/doi/abs/10.1029/2018GL078425` doi: 10.1029/2018GL078425

Mittelholz, A., Johnson, C. L., Thorne, S. N., Joy, S., Barrett, E., Fillingim, M. O., ... Banerdt, W. B. (2020). The Origin of Observed Magnetic Variability for a Sol on Mars From InSight. *Journal of Geophysical Research: Planets*, *125*(9), 1–14. doi: 10.1029/2020JE006505

Mittelholz, A., Johnson, C. L., Thorne, S. N., Yau, V., Joy, S., Barrett, E., ... Others (2021). Magnetic Variations of a Sol Observed Over a Year on Mars with InSight. In *Lunar and planetary science conference* (p. 1941).

Morgan, D. D., Gurnett, D. A., Kirchner, D. L., Fox, J. L., Nielsen, E., & Plaut, J. J. (2008). Variation of the Martian ionospheric electron density from Mars Express radar soundings. *Journal of Geophysical Research: Space Physics*, *113*(9), 1–15. doi: 10.1029/2008JA013313

Nagy, A. F., Winterhalter, D., Sauer, K., Cravens, T. E., Brecht, S., Mazelle, C., ... Trotignon, J. G. (2004). The plasma Environment of Mars. *Space Science Reviews*, *111*(1), 33–114. Retrieved from `https://doi.org/10.1023/B:SPAC.0000032718.47512.92` doi: 10.1023/B:SPAC.0000032718.47512.92

Olsen, N. (1999). Induction studies with satellite data. *Surveys in Geophysics*, *20*(3 - 4), 309–340. Retrieved from `http://dx.doi.org/10.1023/A:1006611303582` doi: 10.1023/A:1006611303582

Olsen, N., Glassmeier, K. H., & Jia, X. (2010). Separation of the magnetic field into external and internal parts. *Space Science Reviews*, *152*(1-4), 135–157. doi: 10.1007/s11214-009-9563-0

Perrin, C., Rodriguez, S., Jacob, A., Lucas, A., Spiga, A., Murdoch, N., ... Banerdt, W. B. (2020). Monitoring of Dust Devil Tracks Around the InSight Landing Site, Mars, and Comparison With In Situ Atmospheric Data. *Geophysical Research Letters*, *47*(10), e2020GL087234. Retrieved from `https://agupubs.onlinelibrary.wiley.com/doi/abs/10.1029/2020GL087234` doi: https://doi.org/10.1029/2020GL087234

Pinçon, J.-L., Menvielle, M., & Szarka, L. (2000). Geomagnetic induction study using the NetLander network of magnetometers. *Planetary and Space Science*, *48*(12), 1261–1270. Retrieved from `https://www.sciencedirect.com/science/article/pii/S0032063300001082` doi: https://doi.org/10.1016/S0032-0633(00)00108-2

Ramstad, R., Brain, D. A., Dong, Y., Espley, J., Halekas, J., & Jakosky, B. (2020). The global current systems of the Martian induced magnetosphere. *Nature Astronomy*. Retrieved from `https://doi.org/10.1038/s41550-020-1099-y` doi: 10.1038/s41550-020-1099-y

Russell, C. T., & Joy, S. P. (2020). InSight IFG Magnetometer Mars Calibrated Data Collection. *NASA Planetary Data System*. doi: https://doi.org/10.17189/1519202

Sagdeev, R. Z., & Zakharov, A. V. (1989). Brief history of he Phobos mission. *Nature*, *341*, 581–585.

Schubert, G., Russell, C. T., & Moore, W. B. (2000). Geophysics: Timing of the Martian dynamo. *Nature*, *408*(6813), 666–667. Retrieved from http://www.nature.com/doifinder/10.1038/35047163 doi: 10.1038/35047163

Smrekar, S. E., Lognonné, P., Spohn, T., Banerdt, W. B., Breuer, D., Christensen, U., ... Wieczorek, M. (2018, dec). Pre-mission InSights on the Interior of Mars. *Space Science Reviews*, *215*(1), 3. Retrieved from https://doi.org/10.1007/s11214-018-0563-9 doi: 10.1007/s11214-018-0563-9

Sonett, C. P. (1982). Electromagnetic induction in the Moon. *Reviews of Geophysics*, *20*(3), 411–455. Retrieved from https://agupubs.onlinelibrary.wiley.com/doi/abs/10.1029/RG020i003p00411 doi: https://doi.org/10.1029/RG020i003p00411

Spiga, A., Murdoch, N., Lorenz, R., Forget, F., Newman, C., Rodriguez, S., ... Banerdt, W. B. (2021). A Study of Daytime Convective Vortices and Turbulence in the Martian Planetary Boundary Layer Based on Half-a-Year of InSight Atmospheric Measurements and Large-Eddy Simulations. *Journal of Geophysical Research: Planets*, *126*(1), 1–28. doi: 10.1029/2020JE006511

Thomas, P., & Gierasch, P. J. (1985). Dust Devils on Mars. *Science*, *230*(4722), 175–177. Retrieved from https://science.sciencemag.org/content/230/4722/175 doi: 10.1126/science.230.4722.175

Thorne, S. N., Johnson, C. L., Mittelholz, A., Langlais, B., Lorenz, R., Murdoch, N., ... Banerdt, W. B. (2022). Investigation of magnetic field signals during vortex-induced pressure drops at InSight. *Planetary and Space Science*, 105487. Retrieved from https://www.sciencedirect.com/science/article/pii/S0032063322000733 doi: https://doi.org/10.1016/j.pss.2022.105487

Thorne, S. N., Mittelholz, A., Johnson, C. L., Joy, S., Liu, X., Russell, C. T., ... Banerdt, W. B. (2020). InSIght fluxgate magnetometer data calibration assessment and implications. In *Lunar and planetary science conference.*

VanderPlas, J. T. (2017). Understanding the lomb-scargle periodogram. *arXiv*, *236*(1), 16. Retrieved from http://dx.doi.org/10.3847/1538-4365/aab766 doi: 10.3847/1538-4365/aab766

Vervelidou, F., Lesur, V., Grott, M., Morschhauser, A., & Lillis, R. J. (2017). Constraining the Date of the Martian Dynamo Shutdown by Means of Crater Magnetization Signatures. *Journal of Geophysical Research: Planets*, *122*(11), 2294–2311. doi: 10.1002/2017JE005410

Vozoff, K. (1991). THE MAGNETOTELLURIC METHOD. In *Electromagnetic methods in applied geophysics: Volume 2, application, parts a and b.* Society of Exploration Geophysicists. Retrieved from https://doi.org/10.1190/1.9781560802686.ch8 doi: 10.1190/1.9781560802686.ch8

Wieczorek, M. A., Broquet, A., McLennan, S. M., Rivoldini, A., Golombek, M., Antonangeli, D., ... Banerdt, W. B. (2022). InSight constraints on the global character of the Martian crust. *Journal of Geophysical Research: Planets*, *n/a*(n/a), e2022JE007298. Retrieved from https://agupubs.onlinelibrary.wiley.com/doi/abs/10.1029/2022JE007298 doi: https://doi.org/10.1029/2022JE007298

Withers, P. (2009). A review of observed variability in the dayside ionosphere of Mars. *Advances in Space Research*, *44*(3), 277–307. Retrieved from http://dx.doi.org/10.1016/j.asr.2009.04.027 doi: 10.1016/j.asr.2009.04.027

Withers, P., & Pratt, R. (2013). An observational study of the response of the upper atmosphere of Mars to lower atmospheric dust storms. *Icarus*, *225*(1), 378–389. Retrieved from https://www.sciencedirect.com/science/article/

979 pii/S0019103513001267 doi: https://doi.org/10.1016/j.icarus.2013.02.032
980 Xu, S., Curry, S. M., Mitchell, D. L., Luhmann, J. G., Lillis, R. J., & Dong, C.
981 (2019). Magnetic Topology Response to the 2003 Halloween ICME Event at
982 Mars. *Journal of Geophysical Research: Space Physics*, *124*(1), 151–165. doi:
983 10.1029/2018JA026118